Available online at www.sciencedirect.com
ScienceDirect
Journal of Nuclear Materials 374 (2008) 320–326
journal of nuclear materials
www.elsevier.com/locate/jnucmat

Iodine isothermal migration behaviour in titanium nitride

S. Gavarini [a,*], H. Jaffrezic [a], P. Martin [b], C. Peaucelle [a], N. Toulhoat [a,1], S. Cardinal [c], N. Moncoffre [a], C. Pichon [a], M. Tribet [a]

[a] IPNL, Université de Lyon, Université Lyon1, CNRS/IN2P3, 4 rue E. Fermi, 69622 Villeurbanne cedex, France
[b] Centre d'études de Cadarache, CEA/DEN/DEC/SESC/LLCC Bâtiment 151, 13108 Saint-Paul-lez-Durance, cedex, France
[c] MATEIS, INSA de Lyon, bât. Blaise Pascal, 20 Avenue A. Einstein, 69621 Villeurbanne cedex, France

Received 17 April 2007; accepted 12 September 2007

Abstract

Titanium nitride is one of the inert matrixes proposed to surround the fuel in gas cooled fast reactor (GFR) systems. These reactors will operate at high temperature and refractory materials with a high chemical stability and good mechanical properties are required. Furthermore, a total retention of the most volatile fission products, such as I, Xe or Cs, by the inert matrix is needed during the in-pile process. The isothermal migration of iodine in TiN was studied by implanting 800 keV I^{++} ions in sintered samples at an ion fluence of 5×10^{15} cm^{-2}. Thermal treatments were performed under secondary vacuum at temperatures ranging from 1200 to 1700 °C. Iodine concentration profiles were determined by 2.5 MeV α-particle elastic backscattering. The migration of iodine seems to be correlated with point defects created by implanted ions near the surface. The Arrhenius plot corresponding to iodine detrapping is curved with possibly two straight-line regions which could indicate either the presence of two types of traps, or a strong dependence of trap's concentration on temperature above 1500 °C. The activation energies associated with each linear region of the Arrhenius plot were found to be: $E_a = 2.4 \pm 0.2$ eV below 1500 °C and $E_{a'} = 11.4 \pm 0.2$ eV above 1500 °C. Nitrogen evaporation from TiN surface under secondary vacuum was proposed as a contributing factor to the enhanced mobility of iodine at high temperature.
© 2007 Elsevier B.V. All rights reserved.

PACS: 66.30.−h; 66.30.−Xj; 51.20.+d; 61.82.Bg; 85.40.Ry

1. Introduction

Within the framework of the Generation IV project, two concepts of gas cooled reactors have been selected: the Very High Temperature Reactor (VHTR) and the Gas cooled Fast Reactor (GFR) [1–4]. In both cases, the fuel will operate at about 1000–1200 °C in normal conditions and may reach 1600–1700 °C in accidental situations. The GFR fuel cycle has to be optimised to recycle actinides and to minimise the waste production. (U, Pu)C carbides and (U, Pu)N nitrides are candidate fuels because of their high densities, decomposition temperatures and thermal conductivities [5,6]. Several geometries for the fuel assembly have been proposed for GFR, prismatic block or pebble bed for example. In each case, the fuel is surrounded by several coating layers and an inert matrix [7,8]. The principal criteria for the choice of the inert matrix are: chemical compatibility with the fuel, mechanical and irradiation resistance, thermal properties allowing high gas temperatures and total retention of fission products (FP) during the in-pile process. The following ceramics have been proposed for core structures in GFR: TiN, ZrN, ZrC, TiC and SiC [5–13].

Titanium nitride is known as a suitable material for the coating of cutting and grinding tools as protection against wear, erosion and chemical attack [14–17]. It is also widely used in microelectronic instrumentation as a diffusion barrier and adhesion promoter between metallic layers [18–21]. The ability of titanium nitride to act as a diffusion barrier combined with its mechanical and thermal properties

* Corresponding author. Tel.: +33 472431464; fax: +33 472448004.
E-mail address: s.gavarini@ipnl.in2p3.fr (S. Gavarini).
[1] CEA/DEN - Saclay, 91191 Gif sur Yvette Cedex.

0022-3115/$ - see front matter © 2007 Elsevier B.V. All rights reserved.
doi:10.1016/j.jnucmat.2007.09.033

make it relevant for the previously described nuclear applications.

Most of the existing studies have been focused on the behaviour of FP, especially rare gases Xe and Kr [22–24], in oxide nuclear fuel in the past four decades and, unfortunately, very few in nitride compounds [25,26]. Xenon thermal migration behaviour in TiN was studied in a previous work and segregation into gas bubbles was shown as a result of xenon low solubility [25]. For iodine, the formation of bubbles several nanometers in size has been demonstrated within UO_2 single crystals that had been implanted with 40 keV ^{127}I ions at a fluence of 10^{16} cm^{-2} and annealed at 1500 °C [27]. Hocking et al. [28] also showed that iodine ions, implanted at the same fluence into polycrystalline UO_2, are associated after thermal treatment with lattice vacancies created by collision cascades during the initial implantation. A concentration threshold of about 10^{16} at cm^{-3} has been determined for iodine trapping in the UO_2 matrix. The aim of the present work is to study the thermally activated migration of iodine implanted into sintered titanium nitride samples at an ion fluence of 5×10^{15} cm^{-2}. The evolution of the concentration profiles will be characterized by Rutherford Backscattering Spectrometry (RBS) as a function of the temperature and the results will be discussed.

2. Experimental

2.1. Sample preparation and thermal treatments

TiN is difficult to densify as a monolithic ceramic due to its high melting point (2950 °C) arising from its strong covalent bonding, nevertheless, few papers report its sintering by conventional sintering [29], hot isostatic pressing (HIP) [30] or hot pressing (HP) [31,32]. Hot pressing (HP) was chosen as sintering process because of the good results reported in literature for TiN samples of simple geometries. A uniaxial pressure of 50 MPa and a progressive increase of the temperature up to 1600 °C were applied to create an initial pellet of 37 mm in diameter and 5 mm in thickness. After cutting, smaller pellets of size $15 \times 15 \times 2$ mm^3 and mean density 5.18 ± 0.01 g cm^{-3} (theoretical density = 5.39 g cm^{-3}, densification about 96%) were obtained. The mean diameter of the grains after sintering was found to be about 18 μm. Samples were polished to micron scale using diamond powders. An open porosity was observed between the grains by Scanning Electron Microscopy (SEM) detecting secondary electrons (Fig. 1(a)), together with some matter wrenching, but no pores were clearly identified in the grains themselves. Impurities were determined by backscattered electrons on polished pellets and were found to be mainly oxygen (homogeneous distribution) with a quantity estimated to about 2 at.% by nuclear resonance ($^{16}O(\alpha, \alpha)^{16}O$ near 3.05 MeV), and elements such as Fe, Ni and Si in the form of inhomogeneously distributed micrometric inclusions (initially present in the powder at a total concentration of a few hundreds of ppm). The annealing procedure was described extensively in a previous work [25], and consists first in pre- and post-implantation thermal treatment at 1000 °C for 10 h in order to anneal most of the damages induced by polishing and ion implantation [33]. In a second stage, higher temperatures are achieved using a 12 kW induction heating system (EFD®). The aim of this second treatment is to induce iodine migration, with temperatures ranging from 1200 to 1700 °C for a few minutes to several hours. For each thermal treatment, the sample is mounted in a silica tube under a vacuum of about 10^{-6} mbar and the temperature is monitored using a bichromatic pyrometer (Impac®). Secondary vacuum was used as external atmosphere to avoid oxidation, however it is worth noting that it could have consequences on the surface stoichiometry of TiN at high temperature through the preferential evaporation of nitrogen [34]. The possible influence of this last process on the implanted species mobility will be discussed further, especially for the highest temperatures performed in this study.

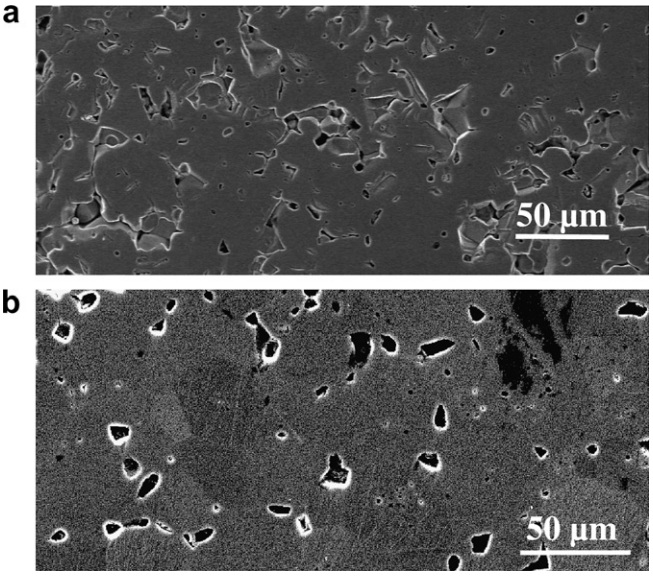

Fig. 1. Secondary electron micrograph of TiN surface: (a) before and (b) after thermal treatment at 1500 °C for 3 h.

2.2. Iodine implantation and RBS analysis

The iodine implantation was performed using a 400 kV accelerator [35] and the implantation energy was 800 keV ($^{127}I^{++}$ ions). The targeted implantation ion fluence was 5×10^{15} cm^{-2} and the ions were implanted under normal incidence at room temperature. The as implanted and post-annealing iodine depth profile distributions were measured by RBS using 2.5 MeV $^4He^+$ incident ions, a detection angle of 172° and a beam intensity of about 10 nA. A typical RBS spectrum of the as-implanted TiN is represented in Fig. 2(a). The iodine peak is located at the high energy side due to its high mass. The experimental range (R_p) and the full width half maximum (FWHM)

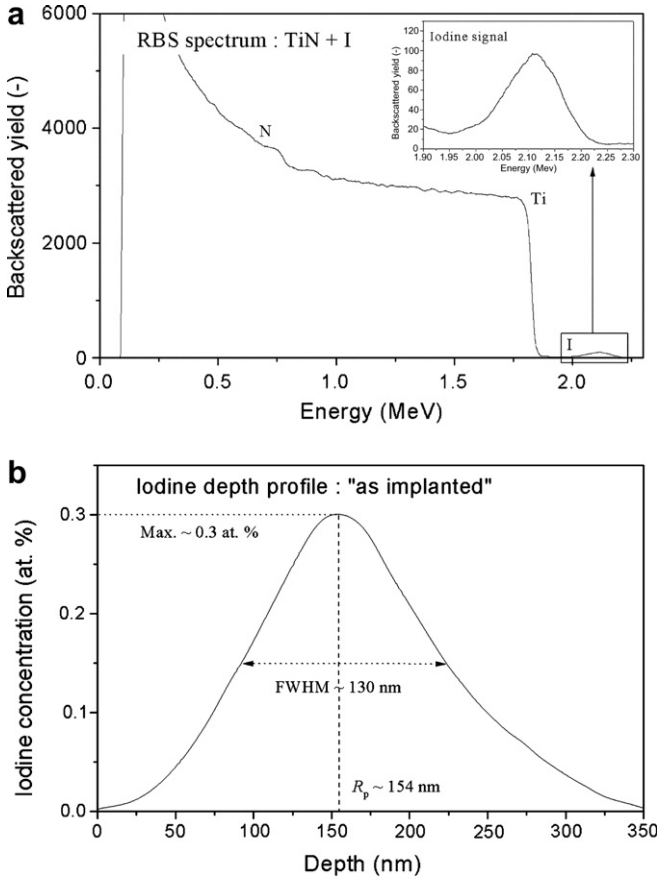

Fig. 2. (a) RBS spectrum of the as implanted TiN sample (α incident particles, 2.5 MeV) and, (b) the corresponding iodine depth profile obtained using SIMNRA® software [36].

are respectively 154 ± 1 nm and 130 ± 1 nm as represented on the depth profile obtained using SIMNRA® software [36] (Fig. 2(b)). The corresponding maximum iodine concentration was found to be about 0.3 at.% at a depth of 154 nm.

3. Results

The surface morphology was observed by SEM, before (Fig. 1(a)) and after thermal treatment (Fig. 1(b)). It remained almost unchanged during thermal treatment with only a slight increase in roughness and in grain boundaries visibility. On the other hand, Fig. 3 represents the modifications of the iodine depth profiles after each thermal treatment. After 27 h at 1200 °C (Fig 3(a)) the signal is shifted to the surface with a slight increase of the full width half maximum of the peak which indicates a weak normal diffusion component. On the contrary, at higher temperature, a slight narrowing of the signal is observed together with an increase of the maximum intensity as shown after 18 h at 1300 °C in Fig. 3(b). This characteristic modification of the profile becomes more evident after 9 h at 1400 °C (Fig. 3(c)) and is associated with a slight shift of the peak maximum position together with a global decrease of the integrated signal. The shift in position indicates a tendency of iodine to diffuse towards the surface and to accumulate particularly at a depth ranging between 140 nm and the initial projected range ($R_p \approx 154$ nm). This accumulation could be the sign of iodine trapping in the near surface region where a high concentration of point defects is likely to remain after initial implantation. The subsequent decrease in the intensity of the peak after 6 h at 1500 °C (Fig. 3(d)) and at higher temperatures (Figs. 3(e)–(g)) indicates a massive release of iodine. The corresponding loss values deduced from the integration of the different signals are summarized in Table 1. The released fraction of iodine varies from 4% at 1200 °C – 27 h to about 10% at 1500 °C – 3 h. For higher temperatures (Figs. 3(e)–(g)), the removal of iodine from the sample varies from 34% at 1600 °C – 30 min to 82% at 1700 °C – ~1 min.

4. Discussion

Fig. 4 shows the distribution of nitrogen vacancy-like defects created by the initial implantation (calculated from SRIM® code [37]) together with the experimental iodine depth profiles before and after thermal treatment at 1500 °C for 3 h. The vacancy concentration is theoretically high in the region between the surface and a depth of about 125 nm corresponding to the maximum defect concentration. It has been shown in many materials that vacancy-like defects created during implantation near the surface constitute potential traps for the implanted species [28,38]. In the case of titanium nitride, the presence of remaining point defects could explain the accumulation of iodine near the surface. In this hypothesis, the driving force associated with the corresponding transport towards the surface during thermal treatment is the energy gain due to the trapping of iodine as it passes from its 'as implanted' position to a more stable trap. The narrowing of the profiles, as it is observed for $T > 1200$ °C, is more enigmatic but the same observation was made by Corni et al. [38] in the case of helium implanted into silicon. Helium is known to be easily trapped in the form of bubbles associated with vacancy-like defects and this last author explained the narrowing and also the delayed release of helium in term of a preferential evacuation of the deeper traps (less energetic) compared to the traps located near the surface. Naturally, this last assumption needs to be confirmed in the case of iodine implanted into titanium nitride because it is still not clear whether iodine is trapped as single atoms or as bubbles/precipitates. The SEM photographs of the surface do not show any visible sign of iodine bubbles after thermal treatment as it was shown for xenon in a previous work [25]. However, the formation and coalescence of nanometric iodine bubbles at depth into defect sites cannot be excluded. This would be the case if a threshold concentration was reached, as observed in UO_2 [28] for which surface trapping of iodine in bubbles was evidenced above a given ion concentration of about 10^{16} cm^{-2}, whereas at lower fluences normal diffusion of atomic species is dominant. In our case, only a slight normal diffusion is observed at

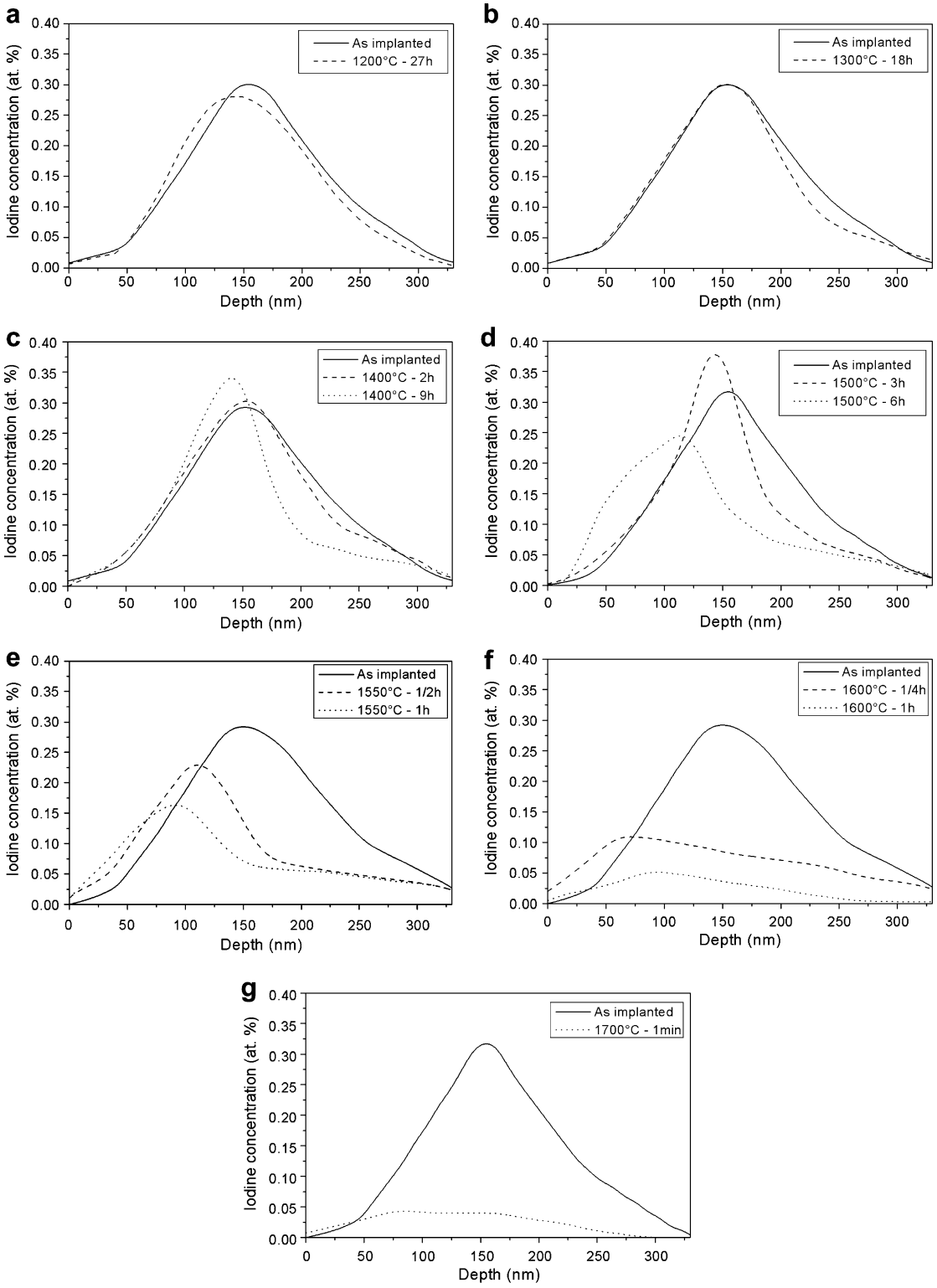

Fig. 3. Iodine depth profile evolution during thermal treatment at: (a) 1200 °C, (b) 1300 °C, (c) 1400 °C, (d) 1500 °C, (e) 1550 °C, (f) 1600 °C and (g) 1700 °C.

1200 °C (Fig. 3(a)), superimposed with a global motion of iodine towards the surface which is consistent with a dominant trapping process near the surface at higher temperature. The equilibrium between the free and the trapped iodine can be written as follow:

$$I_T \leftrightarrow I_U, \tag{1}$$

where I_T and I_U represent respectively trapped and untrapped species. The effect of trapping and detrapping is usually described considering a first order kinetics [39,40]

Table 1
Elemental loss fractions of iodine and calculated values of detrapping time constant k' as a function of temperature

Temperature (K)	Duration (h)	Elemental loss (%)	Detrapping time constant k' (s^{-1})
1473	27	4 ± 1	$4.2 \pm 1 \times 10^{-7}$
1573	18	7 ± 1	$1.1 \pm 0.2 \times 10^{-6}$
1673	2	1 ± 1	/
	9	12 ± 1	$3.9 \pm 0.4 \times 10^{-6}$
1773	3	10 ± 1	/
	6	23 ± 1	$1.2 \pm 0.1 \times 10^{-5}$
1823	0.5	34 ± 1	/
	1	54 ± 1	$2.1 \pm 0.1 \times 10^{-4}$
1873	0.25	49 ± 1	$7.4 \pm 0.1 \times 10^{-4}$
	1	83 ± 1	/
1973	~1 min.	82 ± 2	$2.8 \pm 0.1 \times 10^{-2}$

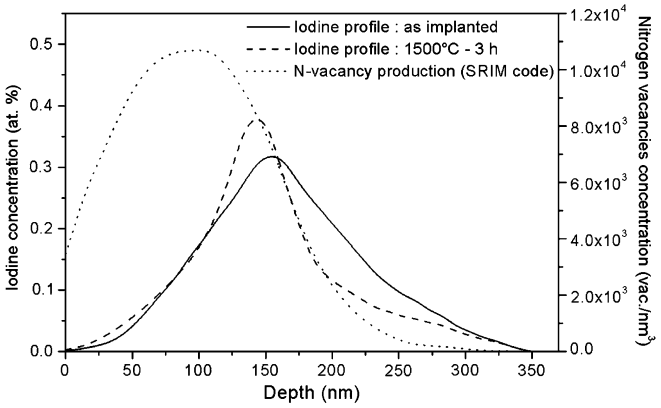

Fig. 4. Nitrogen vacancy distribution after 800 keV iodine implantation at an ion fluence of 5×10^{15} cm^{-2} calculated using SRIM® code [37], together with iodine depth profiles before and after thermal treatment at 1500 °C for 3 h.

$$\frac{dC_T}{dt} = kC_U - k'C_T, \tag{2}$$

where C_T is the concentration of trapped species, C_U the concentration of untrapped species, k the time constant for trapping process (s^{-1}) and k' the time constant for detrapping process (s^{-1}). In our case, the released fraction of iodine was considered, in a first approximation, as the untrapped fraction (I_U) and the remaining iodine fraction was taken as the trapped fraction (I_T). This assumption is supported by the fact that thermal diffusion of iodine into the bulk has not been clearly observed for $T > 1200$ °C, confirming the preponderance of a trapping process. Thus, Eq. (1) cannot be considered as reversible because, in our case, the untrapped species is released very fast and then no more available for trapping process. As a consequence, only the second part of Eq. (2) was considered, resulting in the simplified equation

$$\frac{dC_T}{dt} = -k'C_T, \tag{3}$$

from which

$$C_T = C_0 e^{-k' \times \Delta t}, \tag{4}$$

where, C_T corresponds to the concentration of trapped species trapped after a time Δt at temperature T, and C_0 a pre-exponential factor which can be taken as the initial concentration of trapped species at $t = 0$. Finally, using Eq. (4), the detrapping time constant k' can be expressed as

$$k' = -\frac{\ln\left(\frac{C_T}{C_0}\right)}{\Delta t}. \tag{5}$$

Considering C_T as the remaining concentration of iodine after thermal treatment in the sample and making the assumption that the initially implanted iodine (C_0) is entirely trapped in the host matrix after the post-implantation thermal treatment at 1000 °C – 10 h, the k' values can be calculated using data displayed in Table 1 as a function of the temperature (see Table 1). Using these values, the activation energy associated with iodine detrapping may be estimated assuming a thermally activated time constant [38,39], as expressed in the following equation:

$$k' = k_0 e^{-\frac{E_a}{k_B T}}, \tag{6}$$

where k_0 is a pre-exponential constant, E_a the activation energy (eV) and k_B Boltzmann's constant taken as 8.65×10^{-5} eV K^{-1}. The corresponding Arrhenius plot is represented in Fig. 5 and is curved possibly with two straight-line portions. The slopes associated with each region of the graph were determined and the following activation energy values were calculated: $E_a = 2.4 \pm 0.2$ eV below 1500 °C and $E'_a = 11.4 \pm 0.2$ eV above 1500 °C. The existence of two distinct regions in the Arrhenius plot could have several origins. It is worth noting at this stage that the influence of grain boundaries on the global behaviour of the implanted species is neglected here because of the very small implantation range ($R_p \approx 154$ nm) compared to the mean grain size (about 18 μm), which justify the surface to be considered as the main free surface to be seen by the implanted species. Thus, the first hypothesis to explain the previous non-linearity is the presence of two or more trapping sites, the one with the higher activation energy

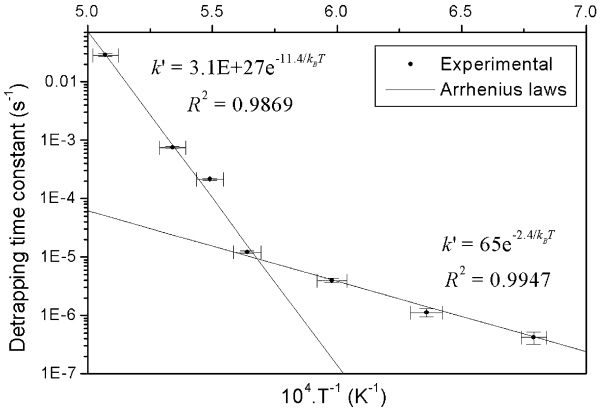

Fig. 5. Representation of the calculated time constant associated with iodine detrapping as a function of temperature together with the corresponding mean Arrhenius laws.

being dominant at high temperature. Another possibility is the existence of a single type of point defects which concentration varies with temperature at high temperature (above 1500 °C) whereas it is constant, or varies much less, at low temperature (below 1500 °C). Even if a combination of both previous processes is possible, the second assumption could be supported by the fact that titanium nitride usually undergoes nitrogen evaporation from the surface at high temperature under vacuum. This last evaporation was extensively described by Gusev et al. [34,41] using the following equation:

$$\mathrm{TiN}_y(s) \rightarrow \mathrm{TiN}_{y_c}(s) + \left[\frac{y - y_c}{2}\right]\mathrm{N}_2(g), \quad (\text{if } y > y_c), \tag{7}$$

where y and y_c are respectively the relative concentration of nitrogen in the initial nitride and in the nitride evaporating congruently at a given temperature. According to Gusev et al., the value of y_c near the surface varies from 0.99 at 1200 °C to about 0.95 at 1600 °C under vacuum. The sub-stoichiometric surface layer reaches its equilibrium after about 1 h and, subsequently, the nitride TiN_{y_c} begins evaporating congruently by the following reaction:

$$\mathrm{TiN}_{y_c}(s) \rightarrow \mathrm{Ti}(g) + (y_c/2)\mathrm{N}_2(g) \tag{8}$$

Once the balance is reached, the high concentration of free octahedral sites near the surface, initially occupied by nitrogen atoms in the fcc structure of TiN, is likely to play a role on iodine mobility and its rapid removal from the sample. It could also contribute to the observed curving of the Arrhenius plot around 1500 °C as nitrogen evaporation starts to be significant above this temperature according to Gusev et al. [34,41]. As an opening to this study, complementary experiments under various pressures of nitrogen in order to control surface stoichiometry could be useful, as Electron–Positron Annihilation (EPA) or Electronic Paramagnetic Resonance (EPR) [42] characterizations for example, to determine the nature of the traps. A more systematic observation of the surface by SEM and TEM will be also carried out to highlight the potential formation of iodine bubbles or precipitates at each stage of the thermal treatments.

5. Conclusion

The thermal migration of iodine implanted into sintered titanium nitride was studied up to 1700 °C under secondary vacuum. A directed diffusion towards the surface was observed followed by an accumulation of iodine at a given depth probably due to trapping in defects created during the initial implantation. Subsequent iodine desorption from traps at high temperature results in a significant release which becomes complete after a few minutes at 1700 °C. The mean activation energies associated with iodine detrapping were found to be 2.4 ± 0.2 eV below 1500 °C and 11.4 ± 0.2 eV above 1500 °C. The existence of two distinct regions in the Arrhenius plot corresponding to iodine detrapping could result from the presence of two types of trapping sites or to a strongly temperature dependant concentration of traps in the high temperature range. This last assumption could be correlated with nitrogen evaporation from the surface under secondary vacuum. These findings may confirm the crucial role played by some structural defect on fission products redistribution within the materials proposed to surround the fuel in present and future nuclear reactors.

Acknowledgments

The authors thank all the people who contributed to this work and especially A. Perrat-Mabilon, A. Gardon, Y. Champelovier and R. Fillol from the 'accelerator group' of the IPNL. Thanks go also to S. Eden for his assistance in English translation.

References

[1] P. Hejzlar, M.J. Pope, W.C. Williams, M.J. Driscoll, Prog. Nucl. Energy 47 (2005) 271.
[2] P. Billot, D. Barbier, in: 2nd International Topical Meeting on High Temperature Reactor Technology, Beijing, China, September 22–24 2004.
[3] http://nuclear.energy.gov.
[4] A technology Roadmap for Generation IV Nuclear Energy Systems, Issued by the US DOE Nuclear Energy Research Advisory committee and the Generation IV International Forum, December 2002.
[5] M. Streit, F. Ingold, J. Eur. Ceram. Soc. 25 (2005) 2687.
[6] K. Minato, M. Akabori, M. Takano, Y. Arai, K. Nakajima, A. Itoh, T. Ogawa, J. Nucl. Mater. 320 (2003) 18.
[7] J. Porta, P. Lo Pinto, M. Bonnet, K. Kugeler, Z. Alkan, R. Heuss, W. von Lensa, Prog. Nucl. Energ. 38 (2001) 407.
[8] C. Guéneau, S. Chatain, S. Gossé, C. Rado, O. Rapaud, J. Lechelle, J.C. Dumas, C. Chatillon, J. Nucl. Mater. 344 (2005) 191.
[9] Y. Arai, K. Nakajima, J. Nucl. Mater. 281 (2000) 244.
[10] N. Chauvin, R.J.M. Konings, Hj. Matzke, J. Nucl. Mater. 274 (1999) 105.
[11] H. Nabielek, W. Schenk, W. Heit, A-W. Mehner, D.T. Goodin, Nucl. Technol. 84 (1989) 62.
[12] K. Minato, T. Ogawa, K. Fukuda, H. Nabielek, H. Sekino, Y. Nozawa, I. Takahashi, J. Nucl. Mater. 224 (1995) 85.
[13] L.C. Walters, D.L. Porter, D.C. Crawford, Prog. Nucl. Energ. 40 (2002) 513.
[14] H.O. Pierson, Handbook of Refractory Carbides and Nitrides, Noyes Publications, 1996.
[15] H.C. Brashilia, A. Jain, K.S. Rajam, Vacuum 72 (2004) 241.
[16] S.A. Barnett, A. Madan, Scr. Mater. 50 (2004) 739.
[17] S. Chatterjee, T.S. Sudarshan, S. Chandrashekhar, J. Mater. Sci. 27 (1992) 1989.
[18] P. Patsalas, S. Logothetidis, J. Appl. Phys. 90 (2001) 4725.
[19] L. Gao, J. Gstöttner, R. Emling, M. Balden, Ch. Linsmeier, A. Wiltner, W. Hansch, D. Schmitt-Landsiedel, Microelectr. Eng. 76 (2004) 76.
[20] Y-H. Shin, Y. Shimogaki, Sci. Technol. Adv. Mater. 5 (2004) 399.
[21] S-K. Rha, W-J. Lee, S-Y Lee, Y-S Hwang, Y-J Lee, D-I Kim, D-W Kim, S-S Chun, C-O Park, Thin Solids Films 320 (1998) 134.
[22] Hj. Matzke, C. Ronchi, C. Baker, Eur. Appl. Res. Rep. Nucl. Sci. Technol. 5 (1984) 1105.
[23] S. Nicoll, Hj. Matzke, C.R.A. Catlow, J. Nucl. Mater. 226 (1995) 51.
[24] V.F. Chkuaseli, Hj. Matzke, J. Nucl. Mater. 201 (1993) 96.
[25] S. Gavarini, N. Toulhoat, C. Peaucelle, J. Mende, Y. Pipon, H. Jaffrezic, P. Martin, J. Nucl. Mater. (2007), doi:10.1016/j.jnucmat.2007.01.239.

[26] Th. Weber, W. Bolse, K.P. Lieb, Nucl. Instrum. and Meth. B 50 (1990) 95.
[27] V.F. Chkuaseli, Hj. Matzke, J. Nucl. Mater. 223 (1995) 61.
[28] W.H. Hocking, R.A. Verrall, I.J. Muir, J. Nucl. Mater. 294 (2001) 45.
[29] O.B. Zgalat-Lozinskii, A.V. Ragulya, V.V. Skorokhod, T.V. Tomila, I.I. Timofeeva, L.I. Klochkov, V.V. Garbuz, Powder Metallurgy and Metal Ceram. 40 (2001) 471.
[30] L. Themelin, M. Desmaison-Brut, M. Boncoeur, F. Valin, L'industrie Céramique 828 (1988) 426.
[31] H. Kuwahara, N. Mazaki, M. Takahashi, T. Watanabe, X. Yang, T. Aizawa, Mater. Sci. Eng. A 319 (2001) 687.
[32] J.R. Groza, J.D. Curtis, M. Kramer, J. Amer. Soc. 83 (2000) 1281.
[33] F. Elstner, H. Kupfer, F. Richter, Phys. Stat. Sol. 147 (1995) 373.
[34] A.I. Gusev, Phys. Stat. Sol. (b) 209 (1998) 267.
[35] http://lyoinfo.in2p3.fr/.
[36] M. Mayer, SIMNRA™ User's guide, Technical report IPP 9/113, 1997, Max Planck Institut für Plasmaphysik Garching.
[37] J.P Biersack, L.G. Haggmark, Nucl. Instrum. and Meth, 257 (1980) 174; http://www.srim.org.
[38] F. Corni, G. Calzolari, S. Frabboni, C. Nobili, G. Ottaviani, R. Tonini, G.F. Cerofolini, D. Leone, M. Servidori, R.S. Brusa, G.P. Karwasz, N. Tiengo, A. Zecca, J. Appl. Phys. 85 (1999) 1401.
[39] J. Philibert, Atom movements, diffusion and mass transport in solids, EDP Sciences, 2006, 578 p.
[40] P.M. Richards, J. Chem. Phys. 92 (1990) 1963.
[41] A.I. Gusev, A.A. Rempel, A.J. Magerl, Disorder an order in strongly non-stoichiometric compounds, transition metal carbides, nitrides and oxides, second ed., Springer, 2006, 628 p.
[42] B. Pivac, B. Rakvin, R. Tonini, F. Corni, G. Ottaviani, Mater. Sci. Eng. B 73 (2000) 60.